Short Article

Structure

The Structure of the Mouse Serotonin 5-HT_3 Receptor in Lipid Vesicles

Graphical Abstract

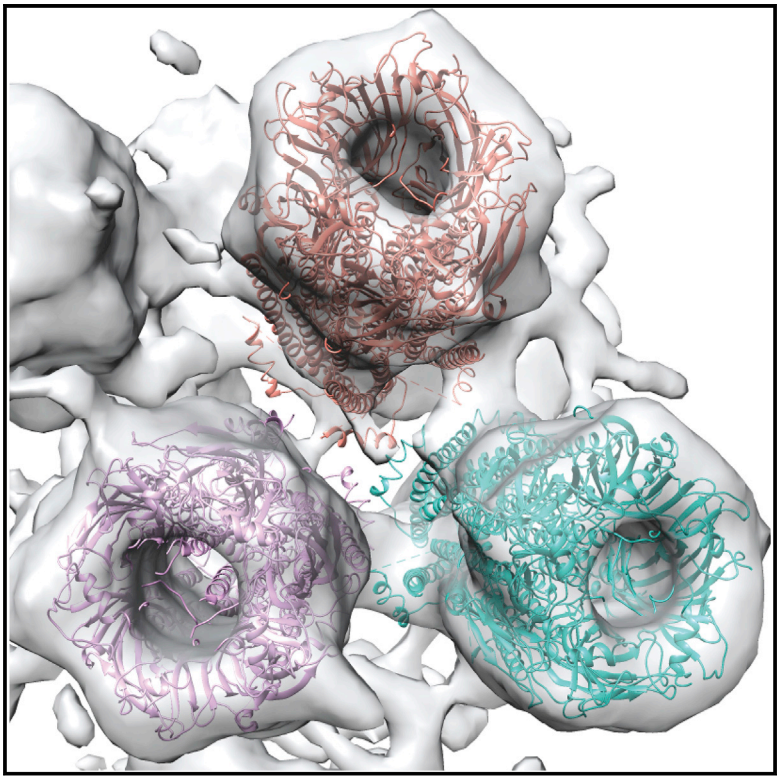

Authors

Mikhail Kudryashev, Daniel Castaño-Díez, Cédric Deluz, ..., Alexandra Graf-Meyer, Horst Vogel, Henning Stahlberg

Correspondence

misha.kudryashev@biophys.mpg.de (M.K.),
horst.vogel@epfl.ch (H.V.)

In Brief

Membrane proteins may change structure in the absence of lipids. A 12-Å resolution structure of a ligand-gated ion channel in a lipid bilayer was obtained by cryo electron tomography. This approach is generally applicable to resolve 3D structures of non-crystalline proteins in membranes.

Highlights

- 5-HT_3 receptors are imaged in lipid bilayers by cryo electron tomography
- Subtomogram averaging resulted in a 3D structure at 12 Å resolution
- No major differences were found between EM and X-ray structures
- Inter-receptor interactions in the membrane are mediated by short horizontal helices

Kudryashev et al., 2016, Structure *24*, 165–170
January 5, 2016
http://dx.doi.org/10.1016/j.str.2015.11.004

Structure
Short Article

The Structure of the Mouse Serotonin 5-HT_3 Receptor in Lipid Vesicles

Mikhail Kudryashev,[1,2,6,*] Daniel Castaño-Díez,[1,3] Cédric Deluz,[4] Gherici Hassaine,[4,7] Luigino Grasso,[4] Alexandra Graf-Meyer,[1,5] Horst Vogel,[4,*] and Henning Stahlberg[1]
[1]Center for Cellular Imaging and NanoAnalytics (C-CINA), Biozentrum, University of Basel, Mattenstrasse 26, 4058 Basel, Switzerland
[2]Focal Area Infection Biology, Biozentrum, University of Basel, Klingelbergstrasse 50/70, 4056 Basel, Switzerland
[3]Scientific Computing Unit, Max Planck Institute for Brain Research, Max-von-Laue-Straße 4, 60438 Frankfurt am Main, Germany
[4]Ecole Polytechnique Fédérale de Lausanne (EPFL), Institute of Chemical Sciences and Engineering (ISIC), Station 6, 1015 Lausanne, Switzerland
[5]Present address: Friedrich Miescher Institute for Biomedical Research, Maulbeerstraße 66, 4002 Basel, Switzerland
[6]Present address: Max Planck Institute for Biophysics, Max-von-Laue-Straße 3, and Buchman Institute for Molecular Life Sciences, Goethe University of Frankfurt, Max-von-Laue-Straße 15, 60438 Frankfurt am Main, Germany
[7]Present address: Theranyx, Grand Luminy Enterprises, Case 922, 163 Avenue de Luminy, 13288 Marseille Cedex 09, France
*Correspondence: misha.kudryashev@biophys.mpg.de (M.K.), horst.vogel@epfl.ch (H.V.)
http://dx.doi.org/10.1016/j.str.2015.11.004

SUMMARY

The function of membrane proteins is best understood if their structure in the lipid membrane is known. Here, we determined the structure of the mouse serotonin 5-HT_3 receptor inserted in lipid bilayers to a resolution of 12 Å without stabilizing antibodies by cryo electron tomography and subtomogram averaging. The reconstruction reveals protein secondary structure elements in the transmembrane region, the extracellular pore, and the transmembrane channel pathway, showing an overall similarity to the available X-ray model of the truncated 5-HT_3 receptor determined in the presence of a stabilizing nanobody. Structural analysis of the 5-HT_3 receptor embedded in a lipid bilayer allowed the position of the membrane to be determined. Interactions between the densely packed receptors in lipids were visualized, revealing that the interactions were maintained by the short horizontal helices. In combination with methodological improvements, our approach enables the structural analysis of membrane proteins in response to voltage and ligand gating.

INTRODUCTION

Membrane proteins perform a variety of vital functions in living organisms, and knowledge of their structure is a prerequisite to understanding their function (Bill et al., 2011; Vinothkumar and Henderson, 2010). Recent developments in direct electron detection and software for single-particle cryo electron microscopy (cryo-EM) allow atomic resolution structures of non-crystalline proteins and protein complexes to be solved (Cheng, 2015). Reports indicate that lipids and detergents affect the conformations of membrane proteins and their mutual interactions (Li et al., 2014; Sun et al., 2015).

High-resolution structures of membrane proteins in lipid bilayers can be obtained by cryo electron crystallography (Abeyrathne et al., 2010). This, however, requires the production of ordered two-dimensional (2D) crystals. An alternative approach is to image non-crystalline membrane proteins in lipid vesicles by cryo electron tomography (cryo-ET) and process the volumes by subtomogram averaging (STA) (Eibauer et al., 2012). Several reconstructions have been obtained at subnanometer resolution (8–9 Å) using this method, namely, for the large stable chaperonin GroEL (Bartesaghi et al., 2012), a large icosahedral virus (Bharat et al., 2015), the structural protein of HIV (Schur et al., 2013), and native virions (Schur et al., 2015). The resolution obtained by cryo-ET and STA is still a critical issue; however, the advantages of direct electron detectors (DEDs) for tomography have so far been exploited to a lesser degree than for single-particle cryo-EM.

Here we concentrate on the serotonin-gated 5-HT_3 receptor (Maricq et al., 1991), which is a pentameric ligand-gated ion channel belonging to the superfamily of Cys-loop receptors (Thompson et al., 2010). The 5-HT_3 receptor is expressed in the CNS in the regions responsible for vomiting, pain, the reward system, cognition, and anxiety control; rodent models suggest that 5-HT_3 receptors are involved in pain perception, emotions, memory, and psychiatric and gastrointestinal disorders (Walstab et al., 2010).

The 3D structure of the detergent-solubilized 5-HT_3 receptor in complex with a high-affinity nanobody, VHH15, has been solved at a resolution of 3.5 Å by X-ray crystallography (Hassaine et al., 2014), which revealed the architecture of the homopentameric receptor, including extracellular, transmembrane, and intracellular domains. The bound nanobody stabilizes a non-conducting channel conformation. Consequently, imaging of the receptor reconstituted in a native-like lipid bilayer in the absence of a restricting nanobody is useful in understanding the physiologically important conformation and the gating mechanism of the receptor.

Here, our aim was to determine the structure of the native, non-crystalline 5-HT_3 receptor in a lipid bilayer. For this we reconstituted the purified, detergent-solubilized receptor in lipid vesicles and performed cryo-ET using direct electron detection

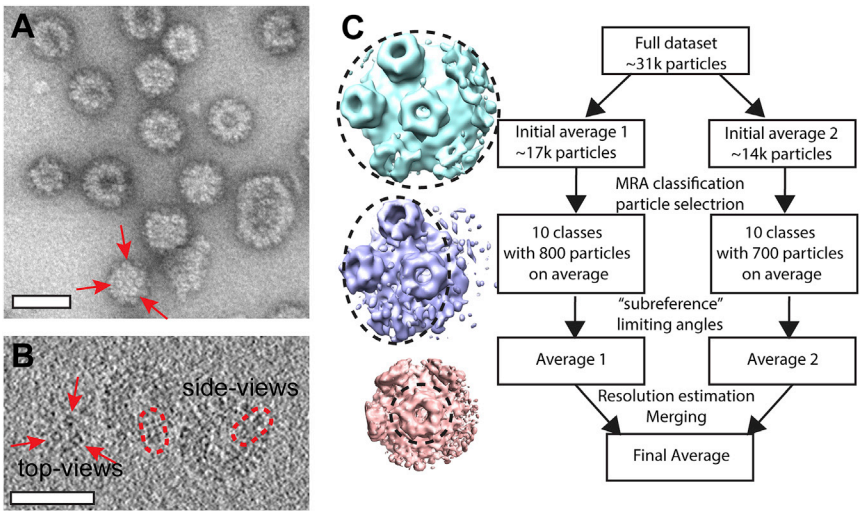

Figure 1. Visualization of 5-HT$_3$ Receptors Densely Packed in the Bilayer of Lipid Vesicles

(A) Lipid vesicles with reconstituted, densely packed 5-HT$_3$ receptors visualized by negative-stain TEM. Single receptors are indicated by red arrows. Scale bar, 50 nm.

(B) An 11-nm thin slice through a low-dose tomogram of the vesicles. Single receptors are marked with red dashed lines (side-views) or indicated by arrows (top-views). Scale bar, 50 nm.

(C) Flow diagram for the deep classification of heterogeneity of the tomographic subvolumes. Top: Initial dataset was split into two half-datasets and initial averages were produced. This was further followed by an MRA classification of the particles in each dataset into ten classes (middle layer) using only the voxels inside a mask containing four neighboring pentamers. At the final step (bottom) the central pentamers from class averages were mutually aligned and averaged, and the final structure was merged from the data of two datasets.

technology. STA of membrane-embedded single-receptor copies combined with deep classification resulted in a structure at 12 Å resolution. The structure showed some secondary structure elements, and also revealed the position of the receptor in the lipid bilayer and preferred contacts between the densely packed receptors. These findings are of physiological relevance, as ligand-gated ion channels are densely packed in the synaptic plasma membranes (Specht et al., 2013).

RESULTS

Purified 5-HT$_3$ receptors were reconstituted into lipid bilayer vesicles of 30–100 nm diameter. Both initial images recorded by negative-stain transmission electron microscopy (TEM) and low-dose cryo-ET reconstructions revealed densely packed receptors in the vesicle bilayers (Figures 1A and 1B). The arrangement of receptors was consistently unidirectional: the smaller cytoplasmic domains were always inside the vesicles and the larger extracellular domains were outside. Single receptors were distinguishable as side- and top-views (Figure 1B).

In total, ~31,000 tomographic subvolumes were extracted from the cryo-ET volumes using a semi-automated routine implemented in *Dynamo* (Castano-Diez et al., 2012). After the initial orientations of the 5-HT$_3$ receptors relative to the membrane had been determined, the particles were separated into two datasets. These datasets were processed independently. A structure was determined for each using the initial angles derived relative to the membrane normal (see Experimental Procedures) and simple refinement steps (Figure 1C). As the signal-to-noise ratio of a single receptor was not sufficient for the particles to be aligned reliably, four neighboring receptors were included in the alignment mask employed. The average of the two resulting structures (Figure 1C, top) had a resolution of ~20 Å and revealed a hexameric arrangement of the receptors on the surface of the vesicles. The same arrangement was observed for densely packed receptors in large, flat membrane patches (Figure S1). Further classification was performed by multi-reference alignment (MRA) into ten classes for each of the two datasets. The classification separated receptor quadruplets according to the curvature of the membrane and the mutual rotation of the receptors to one another. All classes revealed pentameric receptor architecture (Figure 1C, middle). Finally, unbinned class averages including only the first 11 tilt angles from the respective tilt series (0°–30°) were produced for each of the two datasets, i.e., for the low-dose region of the tomograms. Central receptor pentamers were cropped from these class averages and mutually aligned to one another. The two resulting maps gave a final average structure with a resolution of 12 Å (Figures 2A and S2; Movie S1, Table 1). Comparison of the final STA reconstruction with the density map generated from an X-ray structure reported previously for a nanobody-bound and detergent-solubilized receptor (i.e., without the nanobody; Hassaine et al., 2014) showed a significant correlation up to a resolution below 10 Å (Figure S2).

The STA structure clearly reveals the position of the receptor in the lipid bilayer, and defines the position of the membrane for the X-ray structure (Figures 2A and 2B). Transmembrane helices M1–M4 are fully immersed in the lipid bilayer; and short horizontal MX helices seen in the X-ray structure are in our EM structure located at the level of the membrane. The ion permeation pathway is visible in the STA map. (1) The extracellular domain with its internal vestibule is resolved (Hassaine et al., 2014). (2) The transmembrane channel is open over the entire transmembrane region up to the constriction at the interface to the cytoplasmic region (Figures 2D and S2). This is different to the X-ray structure, where the ~5-Å wide constriction of the channel extends from the hydrophobic center toward the cytoplasmic side. This may be due to a limited resolution of the STA map to a different conformation of the transmembrane channel part in the lipid bilayer. (3) On the cytoplasmic side there is a detectable density (Figure 2B, arrow) that is not present in the X-ray structure. Although it seems to bend in the direction of the membrane, unfortunately the STA map does not allow the feature to be traced sufficiently well for building a model.

The relative orientation of the 5-HT$_3$ receptor complexes in the class averages of receptor quadruplets (Figure 1C, top) indicates

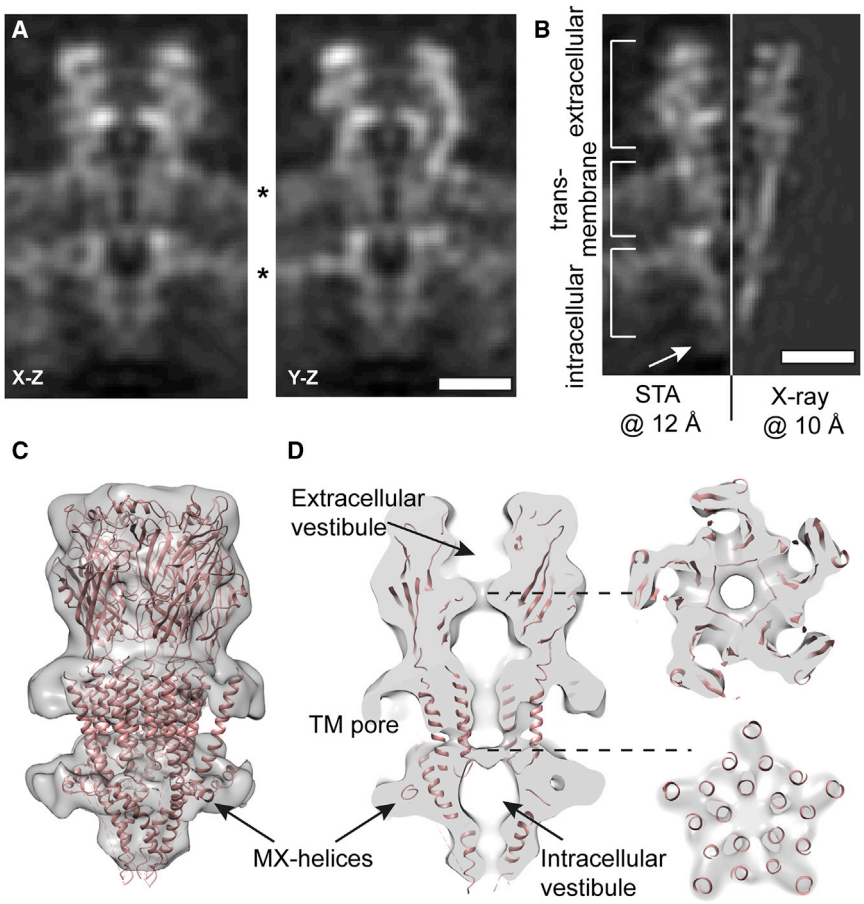

Figure 2. Structure of the 5-HT$_3$ Receptor in the Bilayer of a Lipid Vesicle

(A) A 10-nm thin slice through the STA map of the receptor in lipid vesicles at 12 Å resolution in two viewing directions. Asterisks indicate the lipid bilayer leaflets. Scale bar, 5 nm.

(B) STA map (left) compared with the recalculated X-ray structure at 10 Å resolution (right). The volumes are mutually aligned. The lipid bilayer is visualized as two parallel bright densities projecting from the side of the STA structure. White arrow points to a cytoplasmic density of the STA map that is not present in the X-ray structure. Scale bars for A and B: 5 nm. See also Movie S1 and Figure S2.

(C) A segmented map of the receptor overlaid with the X-ray structure (PDB: 4PIR).

(D) Slices through the segment map in (C) along the dashed lines. The isosurface levels used for the left and right panels are different. TM, transmembrane.

the preferred mutual orientation present in densely packed membranes. Surprisingly, there is a pseudo-C3 arrangement at the interface between the pentamers (Figure 3; Table 1). The short horizontal MX helices (Hassaine et al., 2014) located in the inner membrane leaflet of the neighboring receptors are in close contact with each other in all the class averages. Some class averages have the pseudo-C3 symmetry broken (Figure S3).

Interestingly, the 5-HT$_3$ receptor's high tendency to form densely packed patches in the plasma membrane of living cells (Pick et al., 2003) and in reconstituted lipid bilayers (Figure S1) can be modulated by the lipid composition in the bilayer (Figure S4). In the presence of cholesterol, the 5-HT$_3$ receptor is homogeneously distributed in the bilayer of large unilamellar vesicles; after extraction of cholesterol, the receptor is patched into densely packed membrane regions (Figure S4B). This highlights the importance of investigating membrane protein structure in a native-like lipid environment.

DISCUSSION

Our results demonstrate that cryo-ET and STA can be used to analyze the structure of individual non-crystalline ~250-kDa membrane proteins in lipid membranes. The ~12-Å resolution reconstruction obtained for this homopentameric receptor is, to our knowledge, the highest-resolution structure of a non-crystalline membrane protein in a lipid bilayer. Furthermore, there is a high resemblance to the X-ray structure up to 1 nm resolution, despite the fact that the latter was of crystallized nanobody-bound purified protein in the absence of lipid. Achieving this resolution was made possible by the use of a DED and by adjustments of algorithms for cryo-ET image processing. At this resolution, transmembrane α helices are barely resolved (Figure S2A and Movie S1). Overall the current resolution does not allow reliable understanding of conformational differences between the nanobody-bound X-ray structure and unbound structure in liposomes. This suggests that the scale of conformational changes is low. Structural analysis of a related acetylcholine receptor at 6 Å revealed structural changes associated to ligand binding in the order of ~1 Å (Unwin and Fujiyoshi, 2012). If the conformational changes of 5-HT$_3$ are of similar amplitude, a higher resolution would be needed to visualize it: ~8 Å to visualize movement of alpha helices and ~5.5 Å for β strands of the extracellular domain.

Several critical considerations have to be taken into account if resolutions better than ~12 Å are to be achieved for membrane-embedded structures. First, the use of additional instrumentation for data collection could be implemented, i.e., the addition of an electron energy filter before the DED and the use of a phase plate (Danev et al., 2014); the expected higher signal-to-noise ratio would allow tilt series to be aligned more precisely, overcoming one parameter that is reported to limit the resolution of ET (Voortman et al., 2014). Second, alignment could also be improved by correcting each tilt image for specimen drift (Li et al., 2013); in single-particle EM, this is possible if the DED is operated in the so-called movie mode whereby a series of frames are aligned and summed up to give the final integrated image. Third, the precision of the contrast-transfer function (CTF) correction should be improved; an error in the defocus assignment of 100 nm limits the resolution to about 1 nm under the conditions employed here, as was shown analytically (Zhang and Zhou, 2011) and by direct simulations (Schur et al.,

Table 1. Data Processing Statistics

	5-HT_3 in Lipid Vesicles; EMD-3108
Microscope	FEI Titan Krios
Accelerating voltage (kV)	300
Electron detector	Gatan K2 Summit
Energy filter	none
Angular sampling	[−60:3:60]
Sampling (Å/pixel)	1.67
Defocus range (μm)	−2.5 to −4.5
Total dose (electrons/Å^2)	41
No. of tomograms	46
Software for reconstruction	*WBP* in *IMOD* with *Ctfphaseflip*
Software for STA	*Dynamo*
Particles extracted	~31,000
Asymmetric units in the final reconstruction	~66,500
Resolution (Å)	12.2
Postprocessing	Sharpening

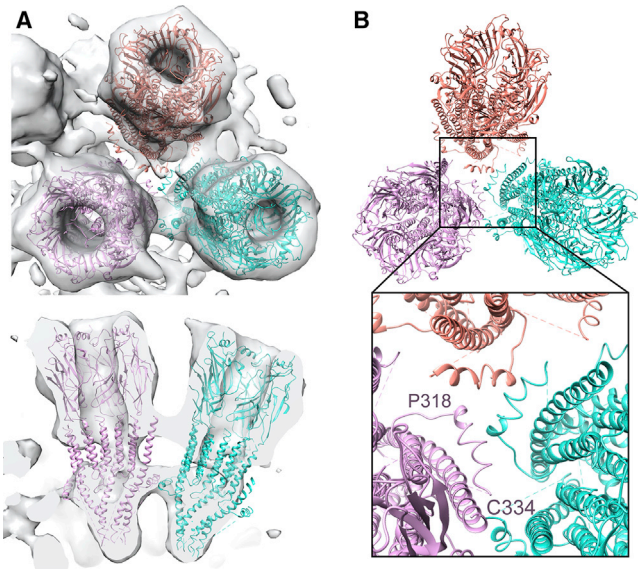

Figure 3. Preferential Interactions between Densely Packed 5HT_3 Receptors in the Bilayer of a Lipid Vesicle

(A) Overlay of a representative class average with three copies of the X-ray structure (4PIR) viewed from top (upper) and side (lower).

(B) Model showing the interaction between MX helices of individual subunits of the three receptors densely packed in the membrane, based on the fit of the X-ray structure to class averages. The distance between the centers of the channels at the height of inner lipid layer is ~60 Å. The lower panel is a magnified view of the indicated region.

See also Figure S3.

2013). One possible way to improve the precision of CTF determination would be to acquire two extra micrographs along the tilt axis for each tilt angle (Eibauer et al., 2012); this approach allowed a structure of the membrane protein MspA to be determined in lipid vesicles at ~17 Å resolution by cryo-ET and STA. Finally, the acquisition of more data should allow a deeper classification of pentamer quadruplets and further improve the resolution. A further major improvement would be to refine the particle alignment parameters using the 2D projections from tilt series rather than the particles from tomographic reconstructions. Such an approach was already implemented for tomograms of isolated GroEL, resulting in an ~8-Å structure revealing secondary structure elements (Bartesaghi et al., 2012). This elegant approach does not have the limitations associated with tilt series reconstructions and could be implementable for general use, in particular for studying membrane proteins inserted in lipids.

Imaging gated ion channels in lipid vesicles in various functional states opens the possibility to image the conformations of the different gating intermediates in a native-like lipid membrane. This may be a particularly powerful way to approach neurotransmitter-gated channels, as the neurotransmitter can be easily added to the buffer outside of the vesicles (Unwin, 2005). If this would allow the determination of an ion channel structure in two different conformational states at a resolution sufficient to distinguish its secondary structure, a mechanistic model for structural consequences of ligand gating might be obtained by flexible fitting with molecular dynamics simulations (Trabuco et al., 2008). Unfortunately, the resolution of the 5-HT_3 receptor presented here is too low to produce a reliable model for the secondary structure.

The classification of the receptors in the densely packed membranes suggested that the 5-HT_3 receptors are positioned in preferred mutual orientations. Interestingly, the 5-HT_3 receptor could be heterologously expressed in mammalian cells at an unprecedentedly high level of about 10 million copies per cell (Pick et al., 2003). Under these conditions the receptors formed densely packed patches of 12,000 receptors/μm^2 in the cells' plasma membranes. Similar densely packed receptors could be formed in artificial lipid membranes and modulated by the lipid composition (Figures S1 and S4).

From heterologous cells submicrometer-sized plasma membrane vesicles could be derived comprising functionally active 5-HT_3 receptors (Pick et al., 2005). It would be interesting to probe whether the horizontal transmembrane MX helices present at the inter-receptor interface significantly affect receptor activity. In our experimental setup, local curvature of the vesicles might have biased receptor-receptor contacts, making contacts at the inner leaflet the determining factor for smaller vesicles (Figure 3A). The same arrangement of the receptors in hexamers might be favored in planar membranes (Figure S1); however the type of contact may be slightly different, as the interactions between extracellular domains will dominate the interaction of receptors and, in addition, could be influenced by the lipid composition of the bilayer. In that case, the accessibility of the 5-HT_3 ligand-binding sites for some large ligands, including VHH15, might be reduced. Thus, the packing of 5-HT_3 receptors in densely packed neuronal membranes should be taken into account during rational drug design.

EXPERIMENTAL PROCEDURES

Protein Production

Protein expression and purification was performed as described previously (Hassaine et al., 2013). The 5-HT_3 receptor obtained was treated with trypsin,

resulting in the cleavage of ~50 residues in the cytoplasmic domain, as reported elsewhere (Hassaine et al., 2014).

Reconstitution of 5-HT_3 Receptor in Small Lipid Vesicles

The concentration of 5-HT_3 receptor was adjusted to 1 mg/ml with dialysis buffer (50 mM Tris [pH 7.5], 120 mM NaCl, 0.01% NaN_3) supplemented with 0.01% Anapoe-C12E9 purchased from Anatrace. Aliquots of the protein solution were mixed with an equal volume of *Escherichia coli* lipids purchased from Avanti Polar Lipids (0.25 mg/ml in 0.5% C12E9) to obtain a final lipid-to-protein ratio of 0.25. The ternary mixtures (total volume: 40 μl) were transferred to dialysis cassettes with a 100-kDa cutoff, purchased from Spectra/Port Biotech. Detergent was removed at room temperature over a period of 1 week. The dialysis buffer was replaced daily.

Negative-Stain Transmission Electron Microscopy

Five-microliter aliquots of diluted samples (reconstituted 5-HT_3 receptor or detergent-solubilized 5-HT_3 receptor) were adsorbed for 60 s to glow-discharged parlodion/carbon-coated copper grids. The grids were then blotted, washed on five drops of double-distilled water, and negatively stained on two droplets of 2% uranyl acetate (pH 4.3) solution. Samples were imaged at a nominal magnifications of 64,000×, 92,000×, or 130,000× using a Philips CM10 electron microscope operated at 80 kV. Electron micrographs were recorded on a 2,048 × 2,048-pixel charge-coupled device camera (Veleta; Olympus Soft Imaging Solutions) mounted in the 35-mm port of the transmission electron microscope, yielding a final pixel size of 1.03, 0.74, or 0.52 nm on the specimen level, respectively.

Cryo electron Tomography

Three microliters of sample supplemented with 5% of 10-nm gold beads were placed on holey carbon grids (Quantifoil Micro Tools), quickly vitrified using a Vitrobot IV (FEI), and imaged at liquid nitrogen temperatures in a Titan Krios (FEI) operated at 300 kV acceleration voltage, using a K2 Summit Direct Electron Detector (Gatan). Tilt series were recorded in counted mode without dose fractionation with an exposure of 1 e/$Å^2$ per image. The final pixel size was 0.167 nm at the specimen level. Tomograms were collected at 3° increments over a 121° range ([0°, 60°] followed by [−3°, −60°]) at a nominal defocus of −2.5 to −4.5 μm. The total electron dose was ~41 electrons/$Å^2$.

Image Processing

Tilt series alignment by gold beads, CTF correction, and 3D reconstruction of unbinned tomograms were performed using *etomo* (Kremer et al., 1996). During manual per-tilt image CTF correction (Xiong et al., 2009), 2–4 Thon rings were observed per micrograph. Particle picking was performed on 2 × 2 times binned and band-pass filtered tomograms. From 94 acquired tomograms, 46 were selected based on the quality of the tomographic alignment. Centers and radii of separate vesicles were manually picked in *imod* (Kremer et al., 1996). Further processing was done with *Dynamo* (Castano-Diez et al., 2012), and particles from the surface of vesicles were automatically extracted based on a vesicle surface triangulation every 8 nm. Approximately 31,000 particles with a box size of ~320 × 320 × 320 Å (a cube comprising 192 × 192 × 192 voxels at 1.67 Å voxel width) were stored on a hard drive. The initial orientations for every particle were determined as a normal vector to the vesicle membrane and stored in a *Dynamo* table. All particles were split into two separate datasets and processed further independently.

Starting averages were generated using the initial orientations. Further refinement was performed with an azimuthal search restricted to 12° and a spacious alignment mask, resulting at an initial 3D reconstruction at a resolution of ~20 Å. Next, deep classification was applied: for each of the dataset MRA into ten classes was performed. The mask used for the classification included four protein pentamers. This was based on the number of pentamers clearly distinguishable in the initial reconstruction. The classification step was performed on 2× binned particles (3.34 Å/pixel), and frequencies up to 16 Å were used for the alignment. Wherever the refined coordinates of two pentamers were closer than 6 nm, one of them was excluded from the average. The classification procedure separated particles according to the curvature of the membrane and the mutual orientation of receptors. The calculation of the MRA was performed on eight Nvidia Tesla C2075 Graphical Processing Units.

Classes were further reconstructed using unbinned data and only the first 11 tilt angles out of 41 (corresponding to 0°–30° and a total electron dose of 11 e/A^2). These class averages were weighted in Fourier space according to the angular distribution of the contributing particles. Central pentameric receptors from nine selected class averages for each dataset were cropped into 128 × 128 × 128-voxel cubes (1.67 Å/voxel). We refer to this process as "sub-reference" generation. Central receptors were fully sampled, and were aligned without missing wedge compensation using a tight mask that only included one protomer C5 symmetry. The resolution was estimated by comparing the two final reconstructions and using a cutoff of 0.143 for the Fourier shell correlation. The final average was calculated as a sum of the two reconstructions and sharpened according to Spiegel et al. (2015). Fitting atomic models into class averages for Figure 3 was done in UCSF Chimera (Pettersen et al., 2004) using the "fit to map" option.

ACCESSION NUMBERS

The 3D reconstruction is deposited at the EMDB with the accession code EMDB: EMD-3108. Unprocessed tilt series are deposited at EMPIAR with the accession code EMPIAR: EMPIAR-10046 (https://www.ebi.ac.uk/pdbe/emdb/empiar/).

SUPPLEMENTAL INFORMATION

Supplemental Information includes Supplementary Experimental Procedures, four figures, and one movie and can be found with this article online at http://dx.doi.org/10.1016/j.str.2015.11.004.

AUTHOR CONTRIBUTIONS

M.K. performed structural analysis and analyzed the results. D.C.D. provided new essential algorithmic tools for STA. C.D. and G.H. expressed and purified the 5-HT_3 receptor. A.G.M. reconstituted receptor into vesicles and performed negative-stain TEM. L.G. expressed and imaged receptor in GUVs. M.K., H.V., and H.S. designed and directed the research and wrote the manuscript.

ACKNOWLEDGMENTS

The authors thank Kenneth Goldie and Bill Anderson for expert technical assistance with electron microscopes, Shirley Müller for critically reading the manuscript and discussions, Gunnar Schroeder and Zhe Wang for valuable discussions, and Marek Basler for support to M.K. at the later stages of the project. This work was in part supported by the Swiss initiative for systems biology SystemsX.ch (grant RTD CINA), the Swiss National Science Foundation (grant SNF 315230_146929 and 205320_144427 to H.S. and grant 31003A-133141 to H.V.), the NCCR TransCure, and the European Community (project SynSignal, grant no. FP7-KBBE-2013-613879).

Received: July 28, 2015
Revised: October 5, 2015
Accepted: November 8, 2015
Published: December 24, 2015

REFERENCES

Abeyrathne, P.D., Chami, M., Pantelic, R.S., Goldie, K.N., and Stahlberg, H. (2010). Preparation of 2D crystals of membrane proteins for high-resolution electron crystallography data collection. Methods Enzymol. *481*, 25–43.

Bartesaghi, A., Lecumberry, F., Sapiro, G., and Subramaniam, S. (2012). Protein secondary structure determination by constrained single-particle cryo-electron tomography. Structure *20*, 2003–2013.

Bharat, T.A., Russo, C.J., Lowe, J., Passmore, L.A., and Scheres, S.H. (2015). Advances in single-particle electron cryomicroscopy structure determination applied to sub-tomogram averaging. Structure *23*, 1743–1753.

Bill, R.M., Henderson, P.J., Iwata, S., Kunji, E.R., Michel, H., Neutze, R., Newstead, S., Poolman, B., Tate, C.G., and Vogel, H. (2011). Overcoming

barriers to membrane protein structure determination. Nat. Biotechnol. *29*, 335–340.

Castano-Diez, D., Kudryashev, M., Arheit, M., and Stahlberg, H. (2012). Dynamo: a flexible, user-friendly development tool for subtomogram averaging of cryo-EM data in high-performance computing environments. J. Struct. Biol. *178*, 139–151.

Cheng, Y. (2015). Single-particle cryo-EM at crystallographic resolution. Cell *161*, 450–457.

Danev, R., Buijsse, B., Khoshouei, M., Plitzko, J.M., and Baumeister, W. (2014). Volta potential phase plate for in-focus phase contrast transmission electron microscopy. Proc. Natl. Acad. Sci. USA *111*, 15635–15640.

Eibauer, M., Hoffmann, C., Plitzko, J.M., Baumeister, W., Nickell, S., and Engelhardt, H. (2012). Unraveling the structure of membrane proteins in situ by transfer function corrected cryo-electron tomography. J. Struct. Biol. *180*, 488–496.

Hassaine, G., Deluz, C., Tol, M.B., Li, X.D., Graff, A., Vogel, H., and Nury, H. (2013). Large scale expression and purification of the mouse 5-HT3 receptor. Biochim. Biophys. Acta *1828*, 2544–2552.

Hassaine, G., Deluz, C., Grasso, L., Wyss, R., Tol, M.B., Hovius, R., Graff, A., Stahlberg, H., Tomizaki, T., Desmyter, A., et al. (2014). X-ray structure of the mouse serotonin 5-HT3 receptor. Nature *512*, 276–281.

Kremer, J.R., Mastronarde, D.N., and McIntosh, J.R. (1996). Computer visualization of three-dimensional image data using IMOD. J. Struct. Biol. *116*, 71–76.

Li, X., Mooney, P., Zheng, S., Booth, C.R., Braunfeld, M.B., Gubbens, S., Agard, D.A., and Cheng, Y. (2013). Electron counting and beam-induced motion correction enable near-atomic-resolution single-particle cryo-EM. Nat. Methods *10*, 584–590.

Li, Q., Wanderling, S., Sompornpisut, P., and Perozo, E. (2014). Structural basis of lipid-driven conformational transitions in the KvAP voltage-sensing domain. Nat. Struct. Mol. Biol. *21*, 160–166.

Maricq, A.V., Peterson, A.S., Brake, A.J., Myers, R.M., and Julius, D. (1991). Primary structure and functional expression of the 5HT3 receptor, a serotonin-gated ion channel. Science *254*, 432–437.

Pettersen, E.F., Goddard, T.D., Huang, C.C., Couch, G.S., Greenblatt, D.M., Meng, E.C., and Ferrin, T.E. (2004). UCSF Chimera—a visualization system for exploratory research and analysis. J. Comput. Chem. *25*, 1605–1612.

Pick, H., Preuss, A.K., Mayer, M., Wohland, T., Hovius, R., and Vogel, H. (2003). Monitoring expression and clustering of the ionotropic 5HT3 receptor in plasma membranes of live biological cells. Biochemistry *42*, 877–884.

Pick, H., Schmid, E.L., Tairi, A.P., Ilegems, E., Hovius, R., and Vogel, H. (2005). Investigating cellular signaling reactions in single attoliter vesicles. J. Am. Chem. Soc. *127*, 2908–2912.

Schur, F.K., Hagen, W.J., de Marco, A., and Briggs, J.A. (2013). Determination of protein structure at 8.5A resolution using cryo-electron tomography and sub-tomogram averaging. J. Struct. Biol. *184*, 394–400.

Schur, F.K., Hagen, W.J., Rumlova, M., Ruml, T., Muller, B., Krausslich, H.G., and Briggs, J.A. (2015). Structure of the immature HIV-1 capsid in intact virus particles at 8.8 A resolution. Nature *517*, 505–508.

Specht, C.G., Izeddin, I., Rodriguez, P.C., El Beheiry, M., Rostaing, P., Darzacq, X., Dahan, M., and Triller, A. (2013). Quantitative nanoscopy of inhibitory synapses: counting gephyrin molecules and receptor binding sites. Neuron *79*, 308–321.

Spiegel, M., Duraisamy, A.K., and Schroder, G.F. (2015). Improving the visualisation of cryo-EM density reconstructions. J. Struct. Biol. *191*, 207–213.

Sun, L., Zhao, L., Yang, G., Yan, C., Zhou, R., Zhou, X., Xie, T., Zhao, Y., Wu, S., Li, X., and Shi, Y. (2015). Structural basis of human gamma-secretase assembly. Proc. Natl. Acad. Sci. USA *112*, 6003–6008.

Thompson, A.J., Lester, H.A., and Lummis, S.C. (2010). The structural basis of function in Cys-loop receptors. Q. Rev. Biophys. *43*, 449–499.

Trabuco, L.G., Villa, E., Mitra, K., Frank, J., and Schulten, K. (2008). Flexible fitting of atomic structures into electron microscopy maps using molecular dynamics. Structure *16*, 673–683.

Unwin, N. (2005). Refined structure of the nicotinic acetylcholine receptor at 4A resolution. J. Mol. Biol. *346*, 967–989.

Unwin, N., and Fujiyoshi, Y. (2012). Gating movement of acetylcholine receptor caught by plunge-freezing. J. Mol. Biol. *422*, 617–634.

Vinothkumar, K.R., and Henderson, R. (2010). Structures of membrane proteins. Q. Rev. Biophys. *43*, 65–158.

Voortman, L.M., Vulovic, M., Maletta, M., Voigt, A., Franken, E.M., Simonetti, A., Peters, P.J., van Vliet, L.J., and Rieger, B. (2014). Quantifying resolution limiting factors in subtomogram averaged cryo-electron tomography using simulations. J. Struct. Biol. *187*, 103–111.

Walstab, J., Rappold, G., and Niesler, B. (2010). 5-HT(3) receptors: role in disease and target of drugs. Pharmacol. Ther. *128*, 146–169.

Xiong, Q., Morphew, M.K., Schwartz, C.L., Hoenger, A.H., and Mastronarde, D.N. (2009). CTF determination and correction for low dose tomographic tilt series. J. Struct. Biol. *168*, 378–387.

Zhang, X., and Zhou, Z.H. (2011). Limiting factors in atomic resolution cryo electron microscopy: no simple tricks. J. Struct. Biol. *175*, 253–263.

